J|A|C|S
ARTICLES
Published on Web 03/19/2005

Dye Sensitization of the Anatase (101) Crystal Surface by a Series of Dicarboxylated Thiacyanine Dyes

S. Ushiroda,[†] N. Ruzycki,[†] Y. Lu,[†] M. T. Spitler,[‡] and B. A. Parkinson*,[†]

Contribution from the Department of Chemistry, Colorado State University, Fort Collins, Colorado 80525, and ChemMotif, 60 Thoreau Street, # 211, Concord, Massachusetts 01742

Received October 1, 2004; E-mail: Bruce.Parkinson@colostate.edu

Abstract: Dye sensitization of the single crystal anatase (101) surface was studied using a structurally similar series of dicarboxylated thiacyanine dyes that bind to the oxide surface through their carboxylate groups. An ultraviolet (UV) light treatment of the anatase (101) surfaces, immediately prior to dye adsorption, improved both the reproducibility of dye coverage and the incident photon-to-current efficiencies (IPCE) for sensitization. The UV treatment does not pit or roughen the anatase surface and results in high IPCEs of more than 1% in some cases and absorbed photon current efficiencies (APCE) from 5 to 100%. The photocurrent spectra showed features associated with surface-bound dye monomers and H-dimers that could be followed as a function of the dye surface coverage. Models for the surface structures of the adsorbed dye layers that are consistent with the measurements are presented, along with a discussion of adsorption isotherms.

Introduction

Dye sensitization of large band-gap semiconductors is the fundamental process that underlies visible light sensitivity in silver halide photography.[1] Photons absorbed by the dyes result in electron transfer to the underlying silver halide substrate to induce latent image formation and eventually the creation of a visual image. This concept was carried over into solar energy research when Tributsch and Calvin[2] peformed studies using chlorophyll to sensitize a ZnO substrate as an inorganic analogue for photosynthesis reaction centers. Many dozen combinations of organic dyes and semiconductor single crystals were subsequently examined, and the principles and problems of such model sensitization systems have been outlined several times.[3−5] Although the inherent limitation of low optical density for a dye monolayer on a single crystal was realized, significant advances in model crystal studies were made with the introduction of nonaqueous solvents and solids with layer-type structures such as WS_2 and SnS_2.[6−9] These changes resulted in the absorbed photon current efficiency (APCE) increasing from near 1% to essentially 100%.

The development of the dye-sensitized solar nanocrystalline solar cell has put a practical form to these model systems and brought renewed interest to the field. The use of nanocrystalline materials allows the optical density of the attached dye layer to be arbitrarily high while the APCE remains near 1. Photovoltaic devices based on nanocrystalline TiO_2 films with adsorbed ruthenium complex sensitizers have been studied for more than a decade and have achieved overall energy conversion efficiencies of greater than 10%.[10]

The most popular sensitizing dye for sensitizing nanocrystalline solar cells is *cis*-di(thiocyanato)-bis(2,2′-bipyridyl-4, 4′-dicarboxylate)ruthenium(II), known as N3. The N3 dye has four pendant carboxyl groups through which it can bind to a planar anatase surface with at least two but up to three bonds.[10] In principle, all four carboxyl groups could be involved in bonding at step, kink, or defect sites. Organic dyes such as cyanines, merocyanines, and squaraine have also been used as sensitizers for nanocrystalline cells.[11−13] These organic dyes adsorbed on semiconductor surfaces could be monomeric, H-, or J-aggregates or a mixture of these forms. Spitler and coworkers[6] have shown that many dicarboxylated cyanine dyes are also effective when used in the nanocrystalline dye-sensitized solar cells. They identified H-aggregates and monomers of these dicarboxylated cyanine dyes in the photocurrent spectra of the nanocrystalline anatase films. The type of dye aggregation present on the surface has important implications for the light absorption and energy conversion efficiency of the cell. The transition moments and the resultant oscillator strength are

[†] Colorado State University.
[‡] ChemMotif.

(1) James, T. H. *The Theory of the Photographic Process*; MacMillian: New York, 1966.
(2) Tributsch, H.; Calvin, M. *Photochem. Photobiol.* **1971**, *14*, 95−112.
(3) Gerischer, H.; Willig, F. *Top. Curr. Chem.* **1976**, *61*, 31−61.
(4) Parkinson, B. A.; Spitler, M. T. *Electrochim. Acta* **1992**, *37*, 943−948.
(5) Miller, R. J. D.; McLendon, G.; Nozik, A.; Schmickler, W.; Willig, F. *Surface Electron-Transfer Processes*; Wiley & Sons: New York, 1995.
(6) Spitler, M. T.; Parkinson, B. A. *Langmuir* **1986**, *2*, 549−553.
(7) Parkinson, B. A. *Langmuir* **1988**, *4*, 967−976.
(8) Takeda, N.; Parkinson, B. A. *Electrochim. Acta* **2000**, *45*, 4559−4564.
(9) Takeda, N.; Parkinson, B. A. *J. Am. Chem. Soc.* **2003**, *125*, 5559−5571.
(10) Nazeeruddin, M. K.; Kay, A.; Rodicio, I.; Humphry-Baker, R.; Muller, E.; Liska, P.; Vlachopoulos, N.; Gratzel, M. *J. Am. Chem. Soc.* **1993**, *115*, 6382−6390.
(11) Law, K.-Y.; Bailey, F. C. *Can. J. Chem.* **1993**, *71*, 494−498.
(12) Bernstein, J.; Goldstein, E. *Mol. Cryst. Liq. Cryst.* **1988**, *164*, 213−216.
(13) Sayama, K.; Tsukagoshi, S.; Mori, T.; Hara, K.; Ohga, Y.; Shinpou, A.; Abe, Y.; Suga, S.; Arakawa, H. *Sol. Energy Mater. Sol. Cells* **2003**, *80*, 47−71.

10.1021/ja044001t CCC: $30.25

associated with the orientation of the dye molecule to the surface as well as to each other and the type of aggregation that the dyes adopt.

H-aggregates show a characteristic blue shift in their absorption spectra relative to the monomer. This blue shift in the spectrum is caused by the arrangement of the stacked dyes, such that the slippage angle (α) that is formed between the parallel transition dipoles and a line joining the centers of the dipoles in the stacked dyes is greater than $\sim$55 °.[14] This noncovalant aggregation of the dyes lowers the degeneracy of the excited state relative to that of noninteracting monomers. In H-dimers, the oscillator strength is completely carried by the higher electronic state, while the transitions to the lower excition state are forbidden.

The dicarboxylated cyanine dyes may covalently bind to the oxide surface through the two carboxylate groups. There has been some discussion in the literature about the binding motif of carboxylates to the anatase surface. An earlier study[15] by Ehret et al. showed that the sensitizing properties of the dyes on nanocrystalline anatase TiO_2 were controlled by the linkage between the dye and the carboxyl functions that attach the dye to the surface. It was noted that monomeric forms of the dyes were seen in some cases, while in others aggregates including dimers were observed adsorbed on the nanocrystalline anatase surfaces. Steric aspects of the dye structures were found to play an important role in this aggregation. Trimethine dyes with ethyl groups substituted at position 9 of the methine aggregate only to the dimer form and not further.[16] Lacking this 9-ethyl substitution, the dyes could aggregate extensively, resulting in a blue-shifted absorption characteristic of an H-aggregate. In contrast, J-aggregation exhibited a red-shifted absorption spectra and the dyes packed close together in either a "herringbone" pattern or a "brick-work"-type pattern on the surface. The ability to control the aggregation of the adsorbed dyes allows for increasing the spectral coverage of a single dye, potentially increasing the efficiency of any device utilizing the dye.

The nanocrystals used in the dye-sensitized solar cells are usually the anatase form of TiO_2 and have predominately (101) orientation. Although efficient and stable solar cells can be made from the dye-sensitized nanocrystalline materials, there has been little fundamental information about the structure or organization of the dyes bound to the metal oxide surface. To date, there have been few studies[17,18] about dye sensitization of the single crystal anatase surface. Herein we use well-characterized, terraced, natural anatase single crystal surfaces as models for the nanocrystalline surface to elucidate aspects of the dye/semiconductor interface. We use a structurally similar series of dyes (Figure 1) to help reveal some details of the dye binding to the surface.

Experimental Section

The crystals used were natural anatase single crystals that were mined in Hargvidda, Tyssedal, in Norway. These bipyramidal crystals exhibited the low-energy growth surfaces with the large wedge-shaped

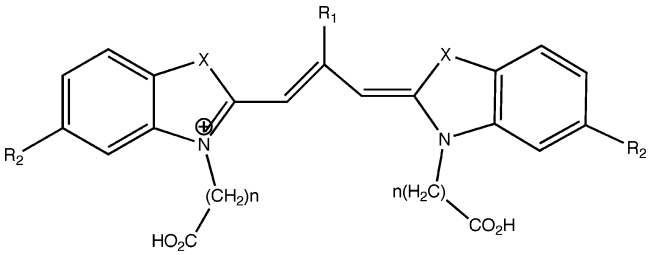

Name	R_1	R_2	X	n
G15	H	H	S	1
G7	C_2H_5	H	S	1
G12	H	CH_3	S	1
G11	C_2H_5	CH_3	S	1
G14	H	OCH_3	S	1
G13	C_2H_5	OCH_3	S	1
B1	H	H	O	0

Figure 1. Structure of the dyes used in this study. The first six, termed G dyes, are considered a structurally similar series, while B1 is a standard for high quantum yields (see text).

(101) faces and the (001) end caps. The (101) crystal faces were dark gray metallic and shiny and were sometimes cut along the (101) plane using a diamond saw, and in other cases entire crystals were used. X-ray photoelectron spectroscopy (XPS) indicated low concentrations of natural impurities including Ca, K, Zr, Zn, and Cl.

Clean terraced surfaces were prepared by polishing the anatase surfaces using 0.02-μm colloidal silica with a soft polishing cloth. The colloidal silica and cloth were obtained from Buehler. The crystals were then annealed at 350 °C for 30 min to remove polishing damage. The surfaces were then examined with atomic force microscopy (AFM) (Digital Instruments nanoscope IIIA controller and a multimode SPM), and when distinct flat single unit cell height terraces were observed, the surface was deemed suitable for dye adsorption studies. The scanning of the surface was performed in air using the tapping mode AFM function. Silicon tips (MikroMasch) with a 40 N/m force constant and 170 kHz resonant frequency were used.

To prepare electrodes for photoelectrochemical studies, the polished anatase (101) surface was rinsed with acetone and sonicated in MilliQ water for 10 min. The anatase sample was then mounted to the electrode, using epoxy (Dexter). After the epoxy set, the electrode was sealed with silicone rubber (RTV) and allowed to dry for a few hours. An ohmic contact was made using Ga/In eutectic (Ga/In=75.5:24.5 by weight) applied to the back of the electrode.

A reproducible surface preparation method was needed to ensure reproducible dye coverages when the electrode was treated in dye solutions. Several methods were tried, but the method that produced the reproducible surfaces is outlined below.

Anatase electrodes were cleaned with 0.2 M NaOH, followed by a MilliQ (18 MΩ) water rinse. Then the anatase was illuminated at 0.6 V versus Ag/AgCl in 1 M HCl for 5 min using an Oriel 150 W Xe lamp followed by an ethanol (Pharmaco, ACS grade) rinse. To allow the UV illumination to reach the sample surface, a quartz cell was used. The photocurrent measured during this treatment was 45−55 μA/cm^2, and the lamp-sample distance was adjusted to achieve this photocurrent. After UV treatment, the electrode was rinsed with ethanol and immediately immersed in a dye solution in ethanol and left for 5 min. High and quite reproducible dye coverages were obtained with this method, and therefore all experiments reported herein used this method. After dye adsorption, the anatase electrode was rinsed with ethanol and then used for the photoelectrochemical measurements. Isotherms were measured by equilibrating the UV-treated anatase electrodes in solutions containing various concentrations of dye for 5 min. The electrode was then cleaned and re-exposed to UV light before being immersed in a solution of the next higher dye concentration.

(14) Tani, T. *Photographic Sensitivity*, 1st ed.; Oxford University Press: New York, 1995; Vol. 8.
(15) Ehert, A.; Stuhl, L.; Spitler, M. T. *Electrochim. Acta* **2000**, *45*, 4553−4557.
(16) Ehert, A.; Stuhl, L.; Spitler, M. T. *J. Phys. Chem. B* **2001**, *105*, 9960−9965.
(17) Kavan, L.; Gratzel, M.; Gilbert, S. E.; Klemenz, C.; Scheel, H. J. *J. Am. Chem. Soc.* **1996**, *118*, 6716−6723.
(18) Fillinger, A.; Soltz, D.; Parkinson, B. *J. Electrochem. Soc.* **2002**, *149*, A1146−1156.

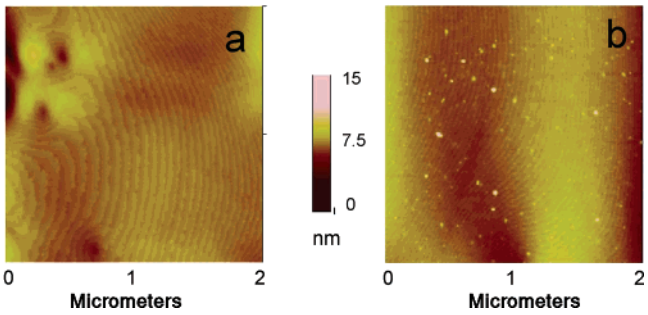

Figure 2. Atomic force microscopy (AFM) images of the anatase (101) surface. (a) The surface after polishing and annealing. The terrace width is ca. 100 nm. (b) The surface of the same crystal as in (a), but after repeated cycles of UV cleaning. White spots seen in the image are attributed to some particulate accumulation after repeated UV cleaning and AFM imaging with laboratory air exposure.

Electrochemical measurements were made in three-electrode configuration with platinum (Pt) counter and Pt pseudo-reference electrode. Acetonitrile (Fisher, optima grade) electrolyte containing 10 mM tetrabutylammonium perchlorate (Fluka, electrochemical grade) was used as a supporting electrolyte with 4.5 mM hydroquinone added as supersensitizer or regenerator. The electrolyte was deoxygenated with nitrogen gas.

Photocurrent/voltage measurements were carried out using potentiostat (EG&G, 174A) and a lock-in amplifier (Stanford Research, SR830) under PC control. Photocurrent spectra were meeasured using an apparatus that has been described previously.[18] The bandwidth of the illuminating light was maintained at 3 nm. An argon ion laser (Ion Laser Technology, model 400) with neutral density filters was used for studying the intensity dependence of the sensitized photocurrent. Measurement of the intensity dependence began at the lowest light intensity, was increased to the highest, and then decreased back to the lowest. The dyes used in this work are depicted in Figure 1 and were prepared through procedures that have been described in previous work.[15]

Incident photon-to-current efficiencies (IPCE) are defined as the ratio of the number of photogenerated electrons collected as photocurrent to the incident photon flux, given by:

$$\mathrm{IPCE}(\%) = \frac{1240 \times j_{\mathrm{photo}}}{\lambda \times I_{\mathrm{o}}} \qquad (1)$$

where j_{photo} is photocurrent in mA/cm^2, l is wavelength in nm, and I_0 is incident photon flux in W/m^2. Photocurrent spectra were analyzed by fitting the monomer and aggregate peak areas using Igor, a commercially available data analysis program, to extract the contributions of monomers, dimers, and aggregates from the spectra after a background subtraction using the multipeak algorithm and Gaussian fitting parameters. The integrated peak areas were used, resulting in a possible error of about 10% in the results, due to the fitting of the small dimer peak at monomer maximum.

Results and Discussion

I. Anatase Surface Preparation. The (101) surface of anatase is a stable[19] and lowest energy surface[20,21] for this TiO_2 polymorph. AFM imaging was used to establish that the anatase surfaces in this study were flat and reproducible through many cleaning, polishing, and dye adsorption cycles. Figure 2a shows an AFM image of terraces obtained from an anatase (101) surface prior to any UV treatment. The image shows terraces with an average width of ca. 100 Å and based on previous experiments,[19] indications of angular step terminations with angle directions of [1$\bar{1}$1] and [1$\bar{1}\bar{1}$] for the cut out angles and [010] for the vertical terrace step edges.

Figure 2b shows an AFM image after repeated cycles of UV treatment similar to what would be experienced by the surface during a normal measurement of a dye-adsorption isotherm where the surface is exposed to various dye concentrations and then cleaned. Essentially no changes in the surface morphology beyond the normal changes in terrace width, observed in all areas of the sample, were observed. Therefore, we conclude that if the UV treatment etches the TiO_2 surface it does so in a layer-by-layer fashion that does not increase the surface area of the sample by pitting or roughening.

Treatment of the anatase surface with band-gap illumination prior to dye adsorption resulted in reproducible dye coverage and relatively short adsorption times. The photogeneration of highly oxidizing holes in the anatase valence band are presumed to be responsible for cleaning any residual impurities from the surface and/or activating the surface for dye adsorption. A kinetic study of the dye adsorption showed that equilibrium coverages could be obtained after 3 min of immersion in dye solutions; however, we routinely used a longer immersion time of 5 min to ensure equilibrium, especially at the lower dye concentrations. This is in contrast to earlier work on N3-based dye adsorption on anatase (101) where many hours were needed to reach an equilibrium coverage[18] presumably due to the need for the dye to displace adsorbed contaminants. In addition, much lower total dye coverages were also measured in the previous work.[18] Higher N3 dye coverages have recently been obtained on anatase (101) by using this procedure.[22]

Repeated cycles between cleaning, sensitization, and photocurrent spectroscopic measurements, using the same electrode and G15 dye solution, resulted in quantum yields that were reproducible at the ±4% level. The photocurrent spectra of the dye-covered electrodes were performed in acetonitrile electrolyte that had no added dye. It was found that the time scale for significant dye desorption was considerably longer than the time needed to run a photocurrent spectrum (ca. 20 min), and therefore we assume some minimal loss of dye during this period, owing to the lack of equilibrium conditions. Detailed studies of the dye desorption process will be presented elsewhere,[23] but it is worthy to note that time-dependent studies showed significant desorption only after >30 min for most of the cyanine dyes adsorbed on the anatase (101) surface.

Information about the electron transfer from the excited state dye to the semiconductor can be deduced from the photocurrent voltage behavior of the sensitized photocurrents. The sensitized photocurrent voltage curves (plotted as IPCE) in Figure 3a for both the G7 and G15 dyes indicate that the photocurrent increases with applied bias from the baseline to a plateau or a slowly increasing plateau value. The photocurrent onset occurs at about −0.4 V and begins to level off at about +0.1 V. Curves taken at the red edge of the photocurrent spectrum (600 nm), where the photocurrent is primarily associated with the monomeric form of the dye, and at the blue edge of the photocurrent

(19) Hebenstreit, W.; Ruzycki, N.; Herman, G. S.; Gao, Y.; Diebold, U. *Phys. Rev. B* **2000**, *62*, R16334−16336.
(20) Lazzeri, M.; Vittadini, A.; Selloni, A. *Phys. Rev. B* **2001**, *63*, 155409−155418.
(21) Lazzeri, M.; Vittadini, A.; Selloni, A. *Phys. Rev. B* **2001**, *65*, 119901 (E).
(22) Ruzycki, N.; Ushiroda, S.; Nelson, J.; Parkinson, B. A., to be submitted for publication.
(23) Ruzycki, N.; Ushiroda, S.; Irby, J.; Lu, Y.; Parkinson, B. A.; Spitler, M. T., to be submitted for publication.

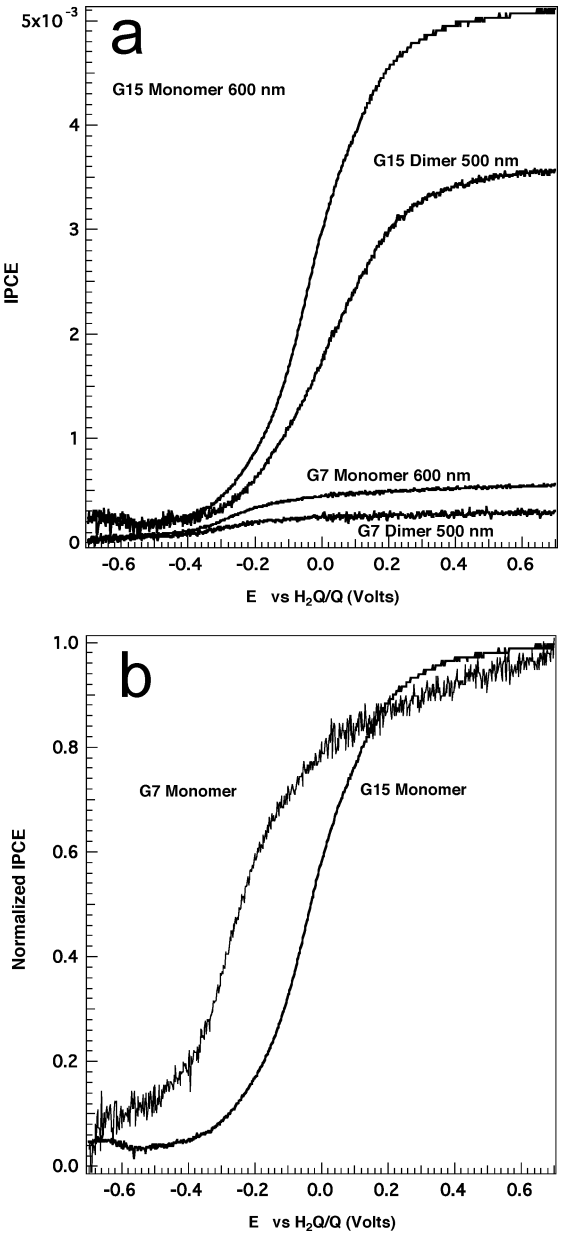

Figure 3. Sensitized photocurrent voltage curves for a 9-ethyl substituted cyanine dye (G7) and a nonbridge substituted dye (G15). (a) The IV curves were taken with illumination at the red (600 nm) and blue (500 nm) sides of the photocurrent spectra corresponding to absorbance by the surface-bound monomers and dimers, respectively. (b) Normalized photocurrent voltage curves for monomers G7 and G15.

spectrum (500 nm), where the photocurrent is associated with the dimeric form of the dye, all have very similar shapes. This indicates that the pathway for electron injection from excitation of monomers and dimers must be similar.

Comparison of the normalized sensitized photocurrent voltage curves (Figure 3b) shows that the smaller photocurrent yield associated with G7 has a 200 mV more negative onset than that for the G15. (The sloping background of the G7 curve has to do with the larger background photocurrent that is magnified when the curves are normalized.) As has been discussed in earlier work, models for dye-sensitized photocurrents predict that the photocurrent should rise to 90% of its plateau value within 59 mV of the flatband potential. This steep onset is not observed with this system or other well-characterized systems,[9] and it implies that electrons transferred by either form of the dye to the TiO_2 surface can recombine with oxidized dye before they can be drawn off as current unless the applied potential is positive enough to produce a large field gradient. One concludes that some form of surface or near-surface traps are involved in the initial electron transfer and that escape from these traps shows only a weak dependence upon potential. All photocurrent spectra reported hereafter are measured at 0.7 V or well into the plateau region of the curves.

II. Dye Adsorption. Since our pretreatment procedure produces reproducible equilibrium dye coverage, we measured the adsorption "isotherms" for the six dyes used in this study adsorbed to the anatase (101) surface. The term isotherm is used here rather loosely since the coverage measurement relies on the assumption that the photocurrent yield is directly proportional to the dye coverage and that the photocurrent yield is the same for all adsorbed dye species. Since there is some small desorption during the experiment, owing to no dye in the test solution, the system is also not under absolute equilibrium conditions needed for a true isotherm. All of the experimental spectra show evidence of both monomers and either dimers or extended aggregates. Because there are multiple species on the surface and because it is not known if these surface species are themselves in equilibrium, interpreting the isotherms is problematic.

Cyanine dyes have been shown[24] to aggregate in solution with many of the thiacyanine dyes exhibiting dimerization with chromophores aligned parallel to each other even at low concentrations, along with a tendency toward H-aggregation at high concentrations. The dimer peaks were blue-shifted between 25 and 60 nm (0.10−0.20 eV) from the monomer peak, and at higher concentrations H-aggregates were observed evidenced by peaks that blue-shifted more than 75 nm (∼0.30 eV) from the monomer species.

The first set of dyes to be discussed will be the 9-ethyl substituted dyes G7, G11, and G13. Figure 4a shows photocurrent (also called action spectra) for the G7 dye obtained after immersion into solutions of increasing G7 concentration from about 0.1 to 400 μM. Absorption spectra show that primarily monomeric dye is present in solution even at higher concentrations used for adsorption of the dye on the plateau region of the isotherm.

All of the 9-ethyl substituted dyes exhibit photocurrent spectra with two peaks: a peak associated with the monomeric dye at ca. 578 nm and a peak associated with dimeric dye that is blue-shifted, indicating a mixture of monomers and dimers on the surface. The monomer and dimer peaks are both sharp and well-defined, with the monomer peak averaging 11 nm in width and the dimer peaks growing in width with increasing coverage and stabilizing at about 30 nm. The spectral shift between the monomer and dimer peaks averages 34 nm in all of the 9-ethyl substituted dyes. The monomer peaks exhibit some red shift from the G7 through the G13 dye due to the addition of electron-withdrawing groups on the dye structure. In G11 there is a methyl group substituted on the phenyl ring of the dye molecule, while on G13 there is a methoxy group.

The blue shift in the action spectra seen for the 9-ethyl substituted dyes is then attributable to the aggregation on the surface. Earlier work with cyanine dyes on nanocrystalline surfaces found that it is unusual to find aggregation of a dye

(24) West, W.; Pearce, S. *J. Phys. Chem.* **1964**, *69*, 1894−1903.

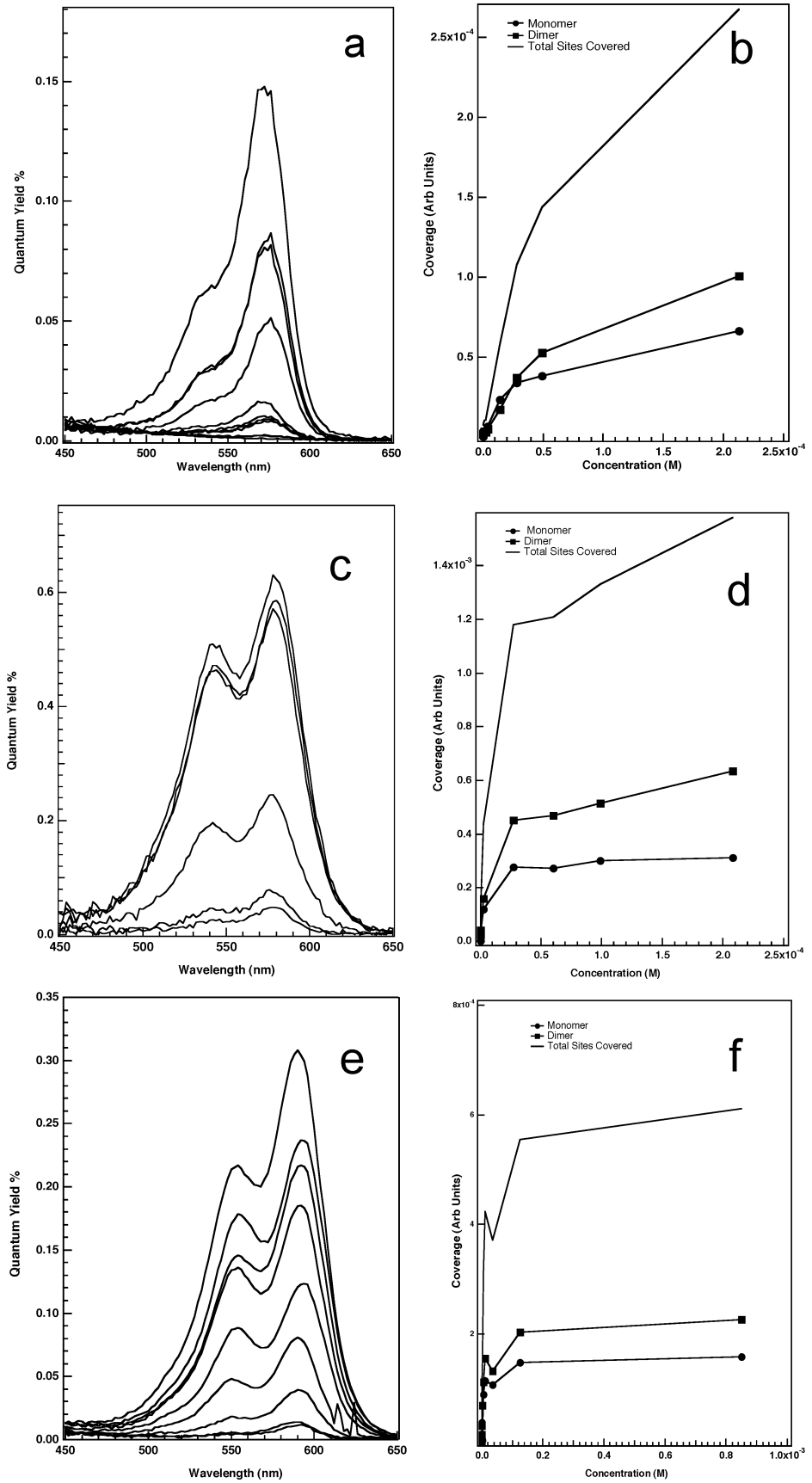

Figure 4. Photocurrent spectra (left) and respective isotherms (right) for the 9-ethyl substituted dyes calculated by integrating the photocurrent spectra. (a) Dye G7 photocurrent spectra at dye concentrations, from bottom curve to top, of 0.12, 0.20, 0.32, 1.2, 2.2, 4.1, 14.0, 28.0, 49.0, and 213 μM. (b) Isotherm for G7. (c) Photocurrent spectra for dye G11 at concentrations, bottom curve to top, of 0.33, 0.41, 2.7, 27.2, 60.4, 99, and 208 μM. (d) Isotherm for G11. (e) Dye G13 photocurrent spectra at dye concentrations, from bottom curve to top, of 0.24, 0.58, 0.97, 2.5, 6.0, 11, 35, 125, and 850 μM. (f) Isotherm for G13.

on surfaces that is limited to dimer formation, such as seen here for the G7, G11 and G13 dyes.[16] It has been suggested that aggregation may be limited if the binding sites for neighboring dyes are separated by a distance larger than the van der Waals interaction distance, requiring a dye pair to "lean toward" each other, thus limiting a close approach of a third molecule. Many studies of noncovalently bound cyanine dyes on surfaces have shown red-shifted or J-aggregation.[16,25−28] The observation of a blue-shifted or H-aggregate type is less well-reported, although at high concentrations in solution these and similar dyes exhibit H-dimerization.[24]

The "isotherm" for G7 illustrated in Figure 4b shows the contributions of dye monomers, dimers, and total adsorbed dye obtained from the fitting of the photocurrent spectrum at the various surface coverages. While the solution spectra show only monomer peaks for the 9-ethyl substituted dyes, the action spectra show that the monomer and dimer peak areas are dependent upon dye coverage. The isotherms reveal that the monomeric form of the dye predominates at low coverages but saturates at a concentration of about 30 μM, whereas the dimer contribution continues to grow in at higher concentrations. Similar trends are observed for the other 9-ethyl substituted dyes, G11 and G13, as seen in Figure 4, parts c and d, respectively.

Similar data for the nonbridge substituted thiacyanine dyes, G15, G12, and G14, are shown in Figure 5a−f. Again, there are two peaks present in the action spectra with a monomer peak and a broader blue-shifted dimer peak. The wavelength of the monomer peaks for the adsorbed dye varied slightly within the nonbridge substituted methine dyes, with the monomer peak ranging from 584 nm in G15 to 598 nm in G14. The average spectral shift between the monomer and the dimer was approximately 40 nm (0.15 eV). The photocurrent peak attributed to the dimer formation tended to broaden with increasing dye concentration, indicating some further aggregation. The dye photocurrent peaks for the extended dimers were approximately 35 nm full width at half-maximum (fwhm) at full dye coverage. While the extended dimer peak showed little shift in the G15 and G12 dyes, it shifted 6 nm toward red in the G14 dye. Peak wavelengths for all dyes studied are summarized in Table 1.

In contrast to the 9-ethyl substituted dyes, where at low dye concentrations the dimer constituted about 30% of the peak area, aggregates of the nonbridge substituted dyes comprised approximately 60% of the total peak area. At higher concentrations, approaching monolayer coverage, the dimer increased to 80% of the peak area, indicating that dimer formation is favored at all coverages for the nonsubstituted dyes. This supports the hypothesis that the less sterically hindered substituted dyes aggregate more easily to a dimer form. In all cases, a small amount of monomer (20−40%) is still present on the surface even at the highest total coverages.

The isotherms for the nonbridge substituted dyes are also characterized by a steeper rise to full coverage, reaching near saturation coverage at less than 30 μM when compared to >30 μM for the bridge substituted dyes. The monomer peak area levels off, while the aggregate peak area continues to rise with increasing concentration.

As mentioned earlier, one must be careful in interpreting the isotherms since multiple species are present on the surface, especially in the case of the aggregating dyes where there could possibly be more than one type of aggregate contributing to the spectrum, and we are operating under the assumption that all dyes have similar photoinjection yields. In all cases, the monomer and dimer contributions to the isotherm were generated directly from the integration of the spectra. The total surface sites covered (Γ_T) was generated by summing the contribution of the monomer (Γ_M) and dimer (Γ_D) as:

$$\Gamma_T = \Gamma_M + 2\Gamma_D \qquad (2)$$

since the dimer peak area is associated with two dye molecules that occupy twice as many surface sites.

The Langmuir isotherm model assumes that the molecules on the surface do not interact. When lateral interaction terms are added to the Langmuir model, attractive interactions create steeper isotherms, while repulsive interactions create less steep isotherms. The shape of the isotherms in Figures 4 and 5 did not fit either a one- or two-site Langmuir isotherm since the dimer-forming dyes exhibit a steep onset indicative of attractive interactions between the adsorbates that are not taken into account in the basic Langmuir model. Modifications of the Langmuir isotherm to allow for a lateral interaction between the molecules have been undertaken using several approaches.[29−32] Monte Carlo methods also allow for inclusion of lateral interactions, as well as for heterogeneous surface interactions. A calculated two-site adsorption isotherm that includes adsorbate interactions has been obtained using Monte Carlo techniques within this group and by others.[33,34] Various isotherms were calculated in an attempt to fit the experimental data, including a Langmuir, Langmuir with lateral interactions, two-site Langmuir adsorption, and Monte Carlo simulation, and these are shown in Figure 6.

A comparison of the calculated and experimental isotherms shown in Figure 6 reveals that sterically hindered dimer-forming dyes (G7) have a less steeply rising isotherm when compared to nonbridge substituted dyes (G15). As seen in Figure 6, it is difficult to choose the best-fit isotherm for the data that have relatively high error bars (±5%). For the 9-ethyl substituted G7 dye, either a Monte Carlo approach with attractive interactions or a two-site adsorption isotherm seems appropriate, but at this point it is mere conjecture to associate a particular calculated adsorption isotherm with the data. What is clear, however, is that these adsorption systems are complex. Features such as the plateau near 2/3 coverage in the isotherm in the repulsive Monte Carlo isotherm is characteristic of a stable ordered structure, and a similar plateau is seen in the G15 case. Energy minima associated with ordered structures are not

(25) Sviridov, D. V.; Shapiro, B. I.; Kulak, A. I. *J. Photochem. Photobiol., A* **1992**, *67*, 377−383.
(26) Kirstein, S.; Steitz, R.; Garbella, R.; Mohwald, H. *J. Chem. Phys.* **1995**, *103*, 818−825.
(27) Li, M.; Wang, A.; Mao, G. *J. Phys. Chem. B* **1999**, *103*, 11161−11168.
(28) Kawasaki, M.; Inokuma, H. *J. Phys. Chem. B* **1999**, *103*, 1233−1241.
(29) Fowler, R. H.; Guggenheim, E. A. *Statistical Thermodynamics*, 1st ed.; Cambridge University Press: Cambridge, 1952.
(30) Aranovich, G. L.; Erickson, J. S.; Donohue, M. D. *J. Chem. Phys.* **2003**, *120*, 5208−5216.
(31) Tarasenko, A. A.; Nieto, F.; Jastrabik, L.; Uebing, C. *Phys. Rev. B* **2001**, *64*, 75413−75430.
(32) Tarasenko, A. A.; Chvoj, Z.; Jastrabik, L.; Nieto, F.; Uebing, C. *Phys. Rev. B* **2001**, *63*, 165423−165434.
(33) Knight, J. N.; Tavener, S.; Szamel, G.; Parkinson, B. A., to be submitted for publication.
(34) Roma, F.; Ramirez-Pastor, A. J.; Ricccardo, J. L. *Langmuir* **2000**, *16*, 9406−9409.

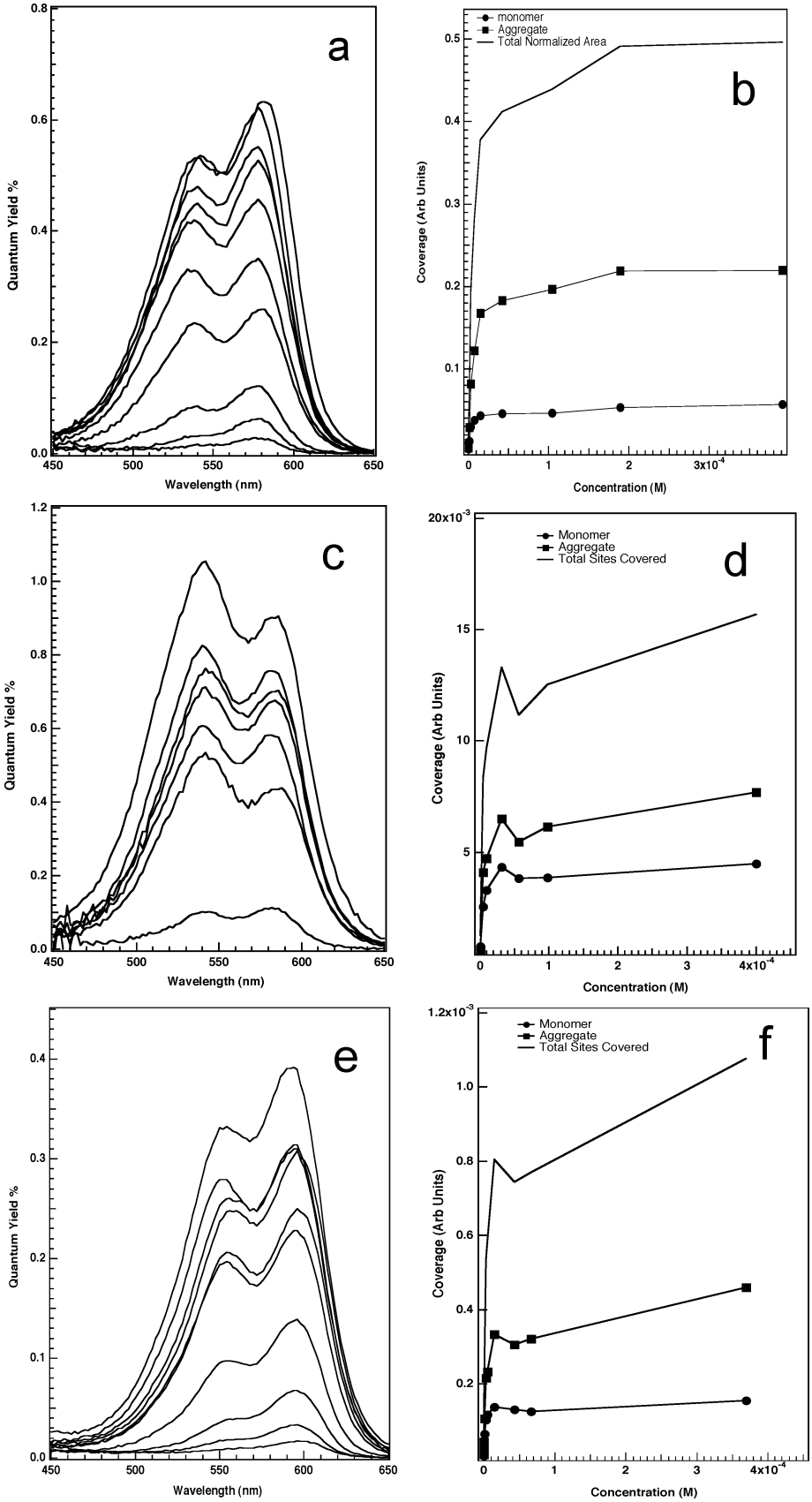

Figure 5. Photocurrent spectra (left) and respective isotherms (right) for the nonbridge substituted dyes calculated by integrating the photocurrent spectra. (a) Photocurrrent spectra for dye G15 at dye concentrations, from bottom curve to top, of 0.22, 0.49, 1.2, 3.2, 7.3, 15.2, 42,104,189, and 391 μM. (b) Isotherm for G15. (c) Dye G12 photocurrent spectra at dye concentrations, from bottom curve to top, of 0.69, 4.5, 10.0, 31.0, 56, 98, and 400 μM. (d) Isotherm for G12. (e) Photocurrrent spectra for dye G14 at dye concentrations, from bottom curve to top, of 0.15, 0.29, 0.49, 1.2, 3.5, 5.3, 15, 43, 67, and 370 μM. (f) Isotherm for G14.

Table 1. Wavelength and Full Width at Half-Maximum (fwhm) for the Monomer and Dimer Species in the Photocurrent Spectra for the Dyes Used in This Study[a]

dye	monomer $\lambda_{(max)}$ (nm)	fwhm (nm)	dimer $\lambda_{(max)}$ (nm)	fwhm (nm)	$IPCE_{(monomer)}$%	$IPCE_{(dimer)}$%
G7	578	11	542	27	0.15	0.06
G11	578	11	544	33	0.65	0.46
G13	594	11	562	30	0.22	0.14
G15	584	13	548	34	0.66	0.48
G12	583	13	542	35	0.70	0.76
G14	598	13	566	35	0.39	0.26

[a] Maximum IPCE values are also noted.

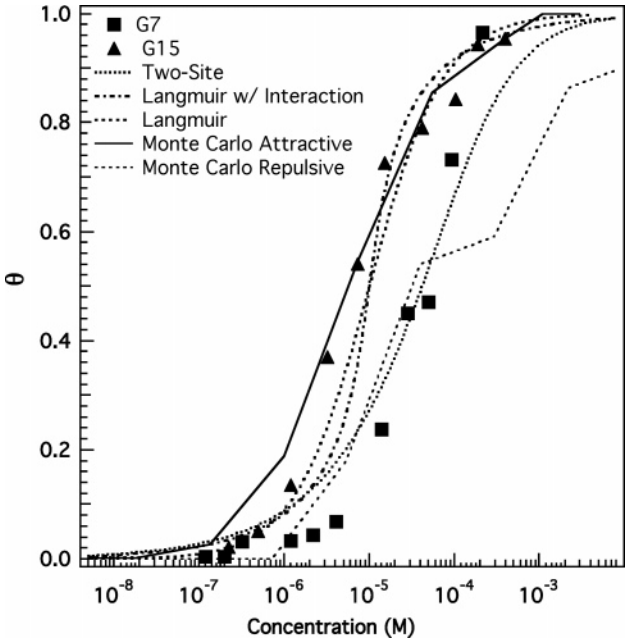

Figure 6. Experimental isotherms for dyes G7 (■) and G15 (▲) plotted with various calculated isotherms.

revealed with simple analytical isotherm expressions, and therefore future work within this group will concentrate on the Monte Carlo technique for fitting and understanding the isotherms for experimental data of this type and obtaining very high quality adsorption data.

III. Proposed Model for Dye Bonding to the Anatase (101) Surface. We turn now to postulating a model for the binding of the dicarboxylated dyes to the anatase (101) surface. It is known[19] that autocompensated anatase (101) has a (1 × 1) surface exhibiting a "sawtooth" profile with ridges of 2-fold coordinated oxygen atoms along the [010] orientation, with the remaining surface and bulk oxygen atoms being 3-fold coordinated. The titanium atoms are 6-fold coordinated in the bulk and 5-fold coordinated (Ti(5)) on the surface. The surface unit cell dimensions are 3.78 Å × 10.24 Å, and while STM images of the surface show wedge-shaped terraces,[19] in this study it will be assumed that the terrace edges are straight for modeling purposes.

Recently, there have been several studies of small molecules bound to both nanocrystalline and single-crystal anatase surfaces.[35−37] UHV studies of methanol and formic acid adsorbed on single crystals of anatase indicate bonding of the oxygens to the Ti(5) sites on the surface.[35,36] Additional UHV studies[35] and theoretical analysis of small molecule adsorbates[38] revealed that water and methanol bind to the surface of anatase in a molecular state, with bonding to the titanium cation site and with hydrogen(s) attaching to the bridging 2-fold oxygens. Because the dyes used in this study contain carboxyl "legs" that attach to the surface, we do not believe that the binding mechanism is significantly different than that observed for similar small molecules with oxygen linkages.

Studies exploring specific dye binding sites, including an IR investigation by Nazeeruddin et al.[39] on the N-series of ruthenium-based dyes on nanocrystalline anatase, indicate that the attachment is via the carboxylic acid groups anchored in a bridging coordination mode. An attachment to the surface using the bridging bidentate mode was also seen to be the most stable binding model in theoretical studies of sodium formate on the anatase (101) surface.[40] A previous study[41] using high-resolution XPS and near-edge X-ray absorption spectroscopy to analyze carboxylic acid adsorption on single crystal rutile (110) indicated that the carboxylate groups are bound to the TiO_2 surface with four equivalent oxygens (two for each carboxylate) to two Ti(5) sites on the surface. An additional study[42] of isonicotinic acid on the surface of rutile (110) corroborated the bridge binding motif and proposed a model of the dye binding that favored dimerization where the molecules "lean" toward each other.

The binding geometry of the carboxylate groups of the cyanine dyes used in this study is still unknown. There have been binding geometries proposed for other dyes with carboxylate "legs"[10,18,43,44] attached to oxide surfaces; however, these have no critical impact on our proposed packing models other than shifting the packing relative to the unit surface cell. As in studies on the adsorption of dye-type molecules on rutile (110)[41,42,45] and the earlier photographic dye work,[46−48] we

(35) Herman, G. S.; Dohnalek, Z.; Ruzycki, N.; Diebold, U. *J. Phys. Chem. B* **2003**, *107*, 2788−2795.
(36) Tanner, R. E.; Liang, Y.; Altman, E. I. *Surf. Sci.* **2002**, *506*, 251−271.
(37) Westermark, K. University of Uppsala, 2003.
(38) Vittadini, A.; Selloni, A.; Rotzinger, F. P.; Gratzel, M. *Phys. Rev. Lett.* **1998**, *81*, 2954−2957.
(39) Nazeeruddin, M. K.; Humphry-Baker, R.; Liska, P.; Gratzel, M. *J. Phys. Chem. B* **2003**, *107*, 8981−8987.
(40) Vittadini, A.; Selloni, A.; Rotzinger, F. P.; Gratzel, M. *J. Phys. Chem. B* **2000**, *104*, 1300−1306.
(41) Patthey, L.; Rensmo, H.; Persson, P.; Westermark, K.; Vayssieres, L.; Stashans, A.; Petersson, A.; Bruhwiler, P. A.; Siegbhan, H.; Lunell, S.; Martensson, N. *J. Chem. Phys.* **1999**, *110*, 5913−5918.
(42) Schnadt, J.; O'Shea, J. N.; Patthey, L.; Schiessling, J.; Krempasky, J.; Shi, M.; Martensson, N.; Bruhwiler, P. A. *Surf. Sci.* **2003**, *544*, 74−86.
(43) Shklover, V.; Haibach, T.; Bolliger, B.; Hochstrasser, M.; Erbudak, M.; Nissen, H.-U.; Zakeeruddin, S. M.; Nazeeruddin, M. K.; Gratzel, M. *J. Solid State Chem.* **1997**, *132*, 60−72.
(44) Matsuura, A. Y.; Obayashi, T.; Kondoh, H.; Ohta, T.; Oji, H.; Kosugi, N.; Sayama, K.; Arakawa, H. *Chem. Phys. Lett.* **2002**, *360*, 133−138.
(45) Schnadt, J.; Schiessling, J.; O'Shea, J. N.; Gray, S. M.; Patthey, L.; Johansson, M. K.-J.; Shi, M.; Krempasky, J.; Ahlund, J.; Karlsson, P. G.; Persson, P.; Martensson, N.; Bruhwiler, P. A. *Surf. Sci.* **2003**, *540*, 39−54.
(46) Bird, G. R.; Norland, K. S.; Rosenhoff, A. E.; Michaud, H. B. *Photogr. Sci. Eng.* **1968**, *12*, 185−195.

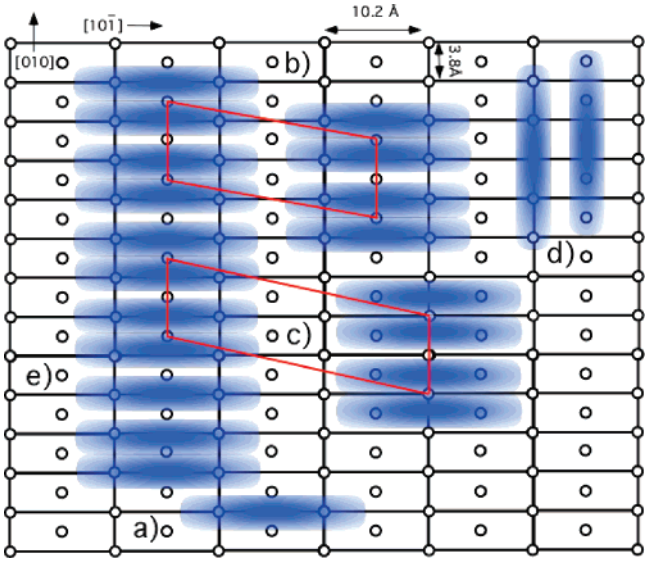

Figure 7. Model of the possible nonbridge substituted dye-packing structures on the anatase (101) surface. The anatase (101) surface unit cells are denoted by the grid. The black circles represent surface five-coordinate Ti atom binding sites. The dyes are depicted as a rectangles. Parts (a) and (e) represent a monomer where (e) is a monomer that is the result of mispairing within a row of dimer pairs. The dark border below (b) represents the smallest dye unit cell for the dimer, which comprises four anatase surface unit cells. The unit cell for (c) comprises six anatase surface cells for rows of dyes going in the [010] direction. The structure near (d) represents structures with the long axis of the dye aligned along the [010] direction that do not have close dimer interactions and would be J-like aggregates.

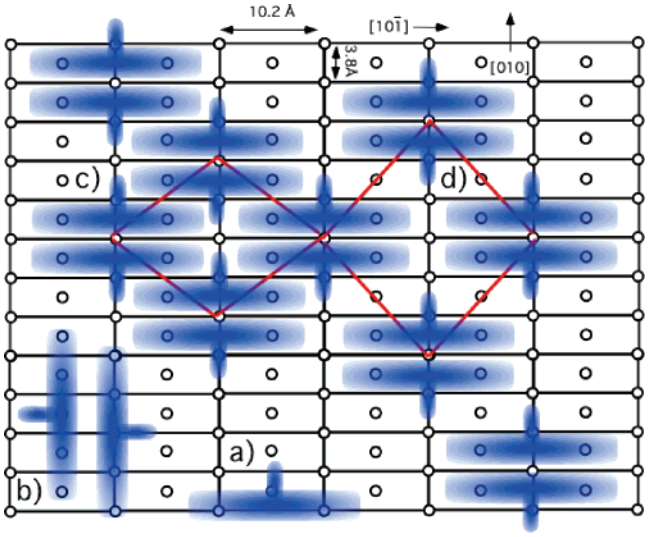

Figure 8. Model of the possible 9-ethyl substituted dye-packing structures on the anatase (101) surface. The anatase (101) surface unit cells are denoted by the grid. The black circles represent surface five-coordinate Ti atom binding sites. The dyes are shown as rectangles, with the 9-ethyl substituent depicted as a flag attached to the rectangle. (a) A monomer that may be attached near a step. (b) J-like dimers. The dark border near (c) represents the smallest dye unit cell for the dimer that comprises four anatase surface unit cells. A less hindered structure is shown in (d) that comprises six anatase unit cells.

believe that the dye binding is influenced by the surface lattice as well as the flexibility (rigidity) of the dye molecules. Through aggregation, by changing the value of the slippage angle (α) or by leaning toward or away from each other, the dyes can optimize their intra- and intermolecular interactions.

In Figures 7 and 8, we present a surface model of the anatase (101), which shows only the Ti(5) surface atoms represented as open circles. Early crystallographic studies[49,50] as well as recent surface experiments[26,51] using cyanine dyes, found that the closest possible "face-to-face" packing of the dye molecules was approximately 3.6 Å, both in solution and on surfaces. Molecular modeling indicates that the distance between the carbon atoms of the two carboxylate groups of our dyes is approximately 7−10 Å, with the total length of the molecule being ~16 Å. We postulate that the two carboxylate "legs" will bind to Ti(5) sites on the surfaces that are separated by close to this 7−10 Å distance. Knowing the distance between the carboxylate groups in the dye as well as the closest "face-to face" distance for the dyes allows us to postulate models of dye aggregation on the surface based on the match of the dye binding groups to the anatase (101) surface lattice. This method was proven useful in early studies of photographic dyes on single crystal surfaces.[46−48] In those studies three assumptions were made that are retained herein:

1. The dyes have ordered epitaxial attachments to the surface.
2. On the basis of crystallographic data, the dyes will tend to maintain an interplanar spacing of ~3.6 Å.
3. The spectral shift of the dye from solution to surface are functions of (a) the dipole matrix element for the electronic transition, (b) the separation of dye chromophores (packing distance), (c) the angular orientation (α) of the chromophores in the aggregate, and (d) the number of molecules in the aggregate.

Figures 7 and 8 show a schematic of the arrangement of the Ti(5) sites on the anatase (101) surface and some possible binding motifs for the dyes used in this study. In Figure 7a−e, several models for the dye orientation for the nonbridge substituted dyes are shown. The monomer is indicated in Figure 7a, with the smallest dimer unit cell shown in Figure 7b. The unit cell for the dye occupies approximately four anatase (101) surface unit cells. Figure 7c shows that the dye may orient with the carboxylate "legs" attached either to the corners of the unit cell or at the centered Ti(5) sites, although this shows a larger dye unit cell area. In both cases, the dyes align along the [101] crystallographic direction. The dye may also align along the [010] direction as seen in Figure 7d, but the intradimer spacing in this case is ca. 5.9 Å, much larger than the optimum dye crystal spacing of 3.6 Å. In addition, the dimers are offset from each other slightly, making them more J-like aggregates than the "head-to-head" orientation of the H-aggregates that are indicated by the spectral response. Finally, Figure 7e shows a dimer pair with a monomer, showing how extended aggregation may occur.

The dye unit cell differs between the dimers formed by the 9-ethyl substituted and nonsubstituted. In the nonsterically hindered dyes, the dyes pack at nearly the minimum intermolecular distance, allowing for some interactions between the sets of dimers. This may be seen in Figure 7b, where the dye unit cell is about four anatase (101) surface unit cells. As the dimers begin to aggregate in extended structures, the spacing between the dimer pairs becomes important for the electronic interactions. We believe the 9-ethyl substituted dyes form only dimer pairs,

(47) Reich, C.; Pandolfe, W. D.; Bird, G. R. *Photogr. Sci. Eng.* **1973**, *17*, 334−342.
(48) Pandolfe, W. D.; Bird, G. R. *Photogr. Sci. Eng.* **1974**, *18*, 340−346.
(49) Booker, L. G. S. *Rev. Mod. Phys.* **1942**, *14*, 275−293.
(50) Sheppard, S. E. *Rev. Mod. Phys.* **1942**, *14*, 303−306.
(51) Chowdhury, A.; Yu, L.; Raheem, I.; Peteanu, L.; Liu, A.; Yaron, D. *J. Phys. Chem. A* **2003**, *107*, 3351−3362.

owing to the steric hindrance of the ethyl substitution spacing of the dimer pairs further apart resulting in less extended interactions. The orientation model for the 9-ethyl substituted dyes is shown in Figure 8. The smallest unit cell for these dyes is a minimum of four anatase (101) surface unit cells as seen in Figure 8a, although this packing is probably not plausible for the sterically hindered dye. A more likely dye unit cell is shown in Figure 8d where the dyes are separated occupying six anatase (101) surface unit cells. The monomer is illustrated in Figure 8a and may also orient in either the [101] or [010] direction. A dimer pair oriented in the [010] direction is shown in Figure 8b where again the intradimer spacing is larger than the planar crystal spacing for the dye. We believe that, in both the substituted and nonsubstituted cyanine dyes, the dimers orient along the [101] direction, epitaxial to the anatase lattice, with a slippage angle (α) approximately 90° to the surface.

While simplistic, this model fits well with previous studies[46−48] of H-aggregating dyes. We regard the presence of only H-type dimers as due to the match between the anatase lattice and the dye dimer pair spacing. If the plane containing the conjugated π-orbital system of the dye is perpendicular to the surface, the flexibility of the methylene carboxylate surface linkage will allow for dimer pairs to "lean" toward each other to achieve the optimum interaction distance found in the solid-state crystal structure (3.6 Å).

The higher IPCE for the nonsubstituted dyes may be attributed to their being more tightly packed on the anatase surface. The monomeric form of the dyes always coexists on the surface with a majority of dimers, as evident in the adsorption isotherms and action spectra at near monolayer coverages. The monomers may exist at domain boundaries between domains of well-ordered dimers such as those shown in Figures 7 and 8, or may be due to defects in the dimer pairing along an axial orientation. In the case of the 9-ethyl substituted dyes, adsorption of a monomer below a step would prevent the dimerization at these sites. In fact, the monomer fraction of bridge substituted dyes is higher than that found for the unsubstituted dyes and correlates with the additional fraction of monomers that would be associated with the number of step edges seen in the AFM images. In addition, it has been proposed[19] that the steps that run in the [010] direction on the anatase (101) surface have titanium atoms that are 4-fold coordinated. If monomers bind to these sites, the site geometry may preclude any dimer or aggregate formation. We are currently conducting studies utilizing dicarboxylated dyes with different carboxylate separations, along with other low index rutile and anatase faces, using scanning probe microscopies to further investigate the proposed dye-packing stuctures. The preliminary AFM results do indicate that the dye molecules cluster and form islands on the anatase surface.

All quantum yield values reported thus far refer to the IPCE. A monolayer of dye only absorbs a small fraction of the incident light; however, it is important to know the photocurrent yield from the absorbed photons, or the APCE, since this number is important for the efficiency of a dye-sensitized solar cell. To calculate the APCE, we used the light harvesting efficiency (LHE), calculated as:

$$\mathrm{LHE} = 1 - 10^{-\mathrm{abs}(\lambda)} \qquad (3)$$

where abs(λ) is the absorption coeficient (ϵ) times the dye coverage. In this study, the extinction coeffiecient was taken from previous experiments to be 1.6×10^5 cm^2/mol-L for monomers and 0.70×10^5 cm^2/mol-L for the dimers.[15,16,24] If the LHE is known, the APCE may be calculated using

$$\mathrm{APCE} = \mathrm{IPCE}/\mathrm{LHE}^{10} \qquad (4)$$

On the basis of the extinction coefficients of the dyes used in this study, a monolayer of these dyes will at best absorb 1−2% of the incident light at the absorption maximum. We use this as a standard to calculate the APCEs of the other dyes from the IPCEs. This approach has been used in previous nanocrystalline studies.[10] For comparison, the APCEs were also calculated by a method used for photographic systems with dyes adsorbed on single crystals of silver halides,[46−48] where the LHE was calculated using eq 3, with the dye coverage determined by using the surface unit cell of the dye and the illuminated area of the crystal. In both these calculations it was assumed that the entire surface was covered by either monomer or dimer. The IPCEs used in the calculations are listed in Table 1, and the calculated APCEs are listed in Table 2, with the first two columns based on a comparison of the highest IPCE obtained by us for any cyanine dye (B1, the oxycyanine equivalent of the thiacyanine dye G15 with no methylene in the attachment chain; Figure 1) on the anatase (101) surface. The next two columns in Table 2 are the results of calculations based on eqs 3 and 4 using the same IPCEs as the first two columns. The highest IPCE values for cyanine dyes adsorbed on the anatase (101) single crystal surface is 1.4% for B1. We performed the APCE calculations, assigning this value to an APCE of 100%.

Both approaches have limitations, mainly not knowing the absolute dye coverage and/or the monolayer absorbance. Therefore, the reported APCEs are at best estimates but are probably underestimates since both calculations are based on the assumption of full monolayer coverage. Near full coverage seems to be achievable with the B1 dye since its IPCE is in the range of the maximum possible value (1−2%). Since the B1 is very similar to the G15 dye, it is difficult to understand why similar coverages are not obtained for both dyes; however, the extra methylene group may give it some additional flexibilty in binding to surface Ti(5) sites. The extra flexibility may also result in a different geometry of the chromophore of the dye with respect to the surface, such as laying down, that may result in stronger coupling of the dye excited state with the semicon-

Table 2. APCE Values Calculated from IPCE Values for the Dyes in This Study (See Text)[a]

dye	APCE (monomer) (%)	APCE (dimer) (%)	APCE (monomer) (%)	APCE (dimer) (%)
	Ethyl on Bridge			
G7	11	5	4	16
G11	45	33	16	70
G13	15	15	4	35
	No Ethyl on Bridge			
G15	40	35	8	40
G12	50	55	9	70
G13	20	20	5	25

[a] The first two columns were calculated on the basis of the IPCEs in Table 1 and ratioed to the maximum IPCE obtained by a cyanine dye (B1) measured on the anatase (101) surface. The second two columns were calculated from eqs 3 and 4, using the area of the dye unit cell as seen in Figures 7 and 8.

ductor surface. Even if one assumes the coverages of the two dyes to be the same, the recombination of injected electrons may differ from dye to dye. One difference between the dyes is that the monomer absorption maximum for B1 is located at 509 nm, about 65 nm blue-shifted from the G15 absorption maximum. This indicates that the HOMO/LUMO gap is 0.27 eV larger for the B1 dye than that for the G15 dye. The HOMO/LUMO gap increase is manifested in the oxidation potential of the B1 dye being 0.15 eV more positive than G15.[16] Previously it was observed that the IPCE for sensitization of SnS_2 by a variety of different dyes was related to the oxidation potential of the dye.[7] No dye sensitization was measured if the oxidation potential of the monomeric dye was located too near the conduction band energy, presumably due to the immediate return of the injected electron into the dye LUMO. Another study comparing sensitization by two squaraine dyes on SnS_2 found a lower quantum yield for the dye with the least positive oxidation potential.[9] Further detailed studies on the relationship between the subtleties of the dye structure, the HOMO/LUMO gap, the oxidation potentials of dyes, and their photosensitization efficiencies on oxide single crystals are currently in progress.[23]

Conclusions

A method of surface preparation and surface activation was developed to produce anatase single crystal (101) surfaces that yield high and reproducible photosensitization yields. Six structurally similar thiacyanine dyes were adsorbed to the anatase (101) surface, and their sensitization behavior was measured. It was found that the isotherms measured for the dyes do not fit well to a simple Langmuir model. IPCEs of up to 1.4% and APCEs from 10 to 100% for the sensitization of single crystal anatase electrodes were achieved, values comparable to nanocrystalline anatase solar cells, demonstrating that at least for some dyes high yields can be reproducibly obtained on metal-oxide single crystal surfaces. The slow rise of the sensitized photocurrent−voltage curves indicates that trapping is probably occurring after electron injection into the conduction band of the anatase crystal and may be involved in recombination pathways that can lower IPCEs and APCEs of some dyes. Models were proposed for the dye ordering on the surface. The dyes tended to form H-dimers, with the nonbridge substituted dyes able to exhibit extended H-dimer interactions and to more efficiently pack the surface, although some monomer was always present on the surface. Structural models with the dyes aligned along the [101] direction of the crystal surface show an alignment consistent with H-type aggregation.

Acknowledgment. This work was supported by the Department of Energy Office of Basic Energy Sciences under Contract No. DE-F603-96ER14625.

JA044001T